

Spin Inertia as a Source of Topological Magnons: Chiral Edge States from Coupled Precession and Nutation

Subhadip Ghosh,¹ Mikhail Cherkasskii,² Ritwik Mondal,¹ Alexander Mook,³ and Levente Rózsa⁴

¹*Department of Physics, Indian Institute of Technology (Indian School of Mines) Dhanbad, IN-826004, Dhanbad, India*

²*Institute for Theoretical Solid State Physics, RWTH Aachen University, 52074 Aachen, Germany*

³*Institute of Solid State Theory, University of Münster, D-48149 Münster, Germany*

⁴*Department of Theoretical Physics, Budapest University of Technology and Economics, H-1111 Budapest, Hungary*

Spin inertia has been demonstrated to give rise to high-frequency nutational excitations beyond the conventional low-frequency precessional modes. Here, we demonstrate that the hybridization between precessional and nutational magnons may give rise to topological phenomena in the spin-wave spectrum. This hybridization requires the presence of interactions breaking angular-momentum conservation, such as the pseudodipolar interaction. We show on the example of a honeycomb ferromagnet how topological gaps open between the precessional and nutational bands that host chiral edge states in slab geometries. Our work establishes a theoretical foundation for exploring inertial spin dynamics as a new route to engineer topological phases in magnetic materials.

The rapid development in the generation of ultrashort laser pulses over the last decades has stimulated studies of magnetization dynamics on femto- to picosecond time scales [1–3]. It has been proposed theoretically that the conventional Landau–Lifshitz–Gilbert (LLG) framework, which accounts for precession and damping, becomes incomplete at these time scales, and has to be extended by an inertial term [4–8]. This spin inertia induces a separation of the directions of the magnetic moment and the angular momentum, causing the former to perform a nutational motion around the latter. In ferromagnetic resonance spectra, spin inertia manifests as a secondary resonance peak appearing typically at terahertz frequencies [9], which has been recently identified experimentally [10–12]. Beyond modifying the linear response, inertial effects also influence spin transport [13], magnetization switching [14], auto-oscillations [15], and the spin-wave dispersion [16–19]. In the latter case, spin inertia results in the doubling of the excitation bands by giving rise to high-frequency nutational spin waves.

The topology of the band structures of spin waves or magnons has also attracted considerable attention recently [20]. Topological magnon insulators with chiral edge modes have been proposed theoretically in multi-sublattice ferromagnets [21–24], magnon crystals [25] and skyrmion lattices [26–28], and magnonic Weyl nodes [29, 30] have also been identified. The topology of the band structure also contributes to transport phenomena such as the magnon thermal Hall effect [31–34]. A prototypical example of a topological magnon insulator is a ferromagnet on a honeycomb lattice, realized in, e.g., chromium trihalides and Cr(Si/Ge)Te₃ compounds [35–37]. Two different microscopic mechanisms have been put forward that could explain the topologically non-trivial nature of the band structure in this structure: the Dzyaloshinsky–Moriya interaction [35, 36, 38, 39] which is antisymmetric in the lattice sites, and various forms of the symmetric two-site exchange anisotropy including dipolar, pseudodipolar, and Kitaev terms [40–42]. It has

been suggested that the Dzyaloshinsky–Moriya interaction may be more prominent in the opening of a gap in the band structure [43], since the gap size scales linearly with its strength but quadratically with the pseudodipolar term. Due to their different symmetry properties, it was also proposed that the two contributions may be distinguished by measuring the magnon spectrum for different orientations of the magnetization [44].

Here, we present how spin inertia influences the topology of the magnon band structure. As an example, we demonstrate that the precessional and nutational magnon bands may hybridize in a honeycomb ferromagnet, leading to an additional gap opening in the spectrum. This hybridization is enabled by the pseudodipolar interaction but not by the Dzyaloshinsky–Moriya interaction, enabling to distinguish between these two contributions, and the gap size is shown to scale linearly with the interaction strength. We confirm the topological nature of this gap by demonstrating the emergence of edge modes in slab geometries, and connect this to the Chern numbers of the bands.

The dynamics of the spins is described by the inertial Landau-Lifshitz-Gilbert (iLLG) equation [4],

$$\dot{\mathbf{S}}_i = \mathbf{S}_i \times \left[-\gamma \mathbf{B}_i^{\text{eff}} + \alpha \dot{\mathbf{S}}_i + \eta \ddot{\mathbf{S}}_i \right]. \quad (1)$$

Here, \mathbf{S}_i denotes a unit vector at site i corresponding to the direction of the magnetic moment, γ is the gyromagnetic ratio, α represents the Gilbert damping constant, and η is the inertial relaxation time. The effective magnetic field is expressed as $\mathbf{B}_i^{\text{eff}} = -\frac{1}{M_i} \frac{\partial \mathcal{H}}{\partial \mathbf{S}_i}$, where \mathcal{H} is the Hamiltonian of the system and M_i is the magnetic moment. The angular momentum at site i may be defined as $\mathbf{L}_i = \frac{M_i}{\gamma} (\mathbf{S}_i - \eta \mathbf{S}_i \times \dot{\mathbf{S}}_i)$ [8], see the Supplemental Material [45]. In the absence of an external magnetic field and spin-orbit coupling, the system is invariant under global rotations, which leads to the conservation of the total angular momentum $\sum_i \mathbf{L}_i$.

To calculate the magnon excitations within linear spin-wave theory, first an equilibrium spin configuration is sought which satisfies $\mathbf{S}_i^{(0)} \times \mathbf{B}_i^{\text{eff}} = \mathbf{0}$ at all lattice sites. Expanding Eq. (1) in small spin deviations $\mathbf{S}_i^\perp = [S_i^-, S_i^+] = [\tilde{S}_i^x - i\tilde{S}_i^y, \tilde{S}_i^x + i\tilde{S}_i^y]$, where in equilibrium $\tilde{S}_i^z = 1$ at all sites in the local frames of reference, yields (cf. Ref. [18])

$$\omega \begin{bmatrix} \mathbf{S}^\perp \\ \mathbf{V}^\perp \end{bmatrix} = \begin{bmatrix} 0 & \mathbb{1} \\ \frac{\gamma}{\eta} \mathbf{M}^{-1} \mathcal{H}_{\text{SW}} & \frac{\sigma^z}{\eta} + i\frac{\alpha}{\eta} \mathbb{1} \end{bmatrix} \begin{bmatrix} \mathbf{S}^\perp \\ \mathbf{V}^\perp \end{bmatrix} = \mathcal{D} \begin{bmatrix} \mathbf{S}^\perp \\ \mathbf{V}^\perp \end{bmatrix}, \quad (2)$$

where $\mathbf{V}^\perp = -i\dot{\mathbf{S}}^\perp$ is the spin velocity, \mathcal{H}_{SW} is the spin-wave Hamiltonian, $\mathbb{1}$ is the unit matrix, \mathbf{M} is a diagonal matrix containing the magnetic moments, and σ^z acts as a Pauli matrix on the two components of \mathbf{S}^\perp . We substituted the harmonic time dependence $\mathbf{S}^\perp \propto e^{i\omega t}$, and replaced the time derivatives with multiplication by $i\omega$. The spin waves correspond to the eigenmodes of the matrix \mathcal{D} in Eq. (2). The magnon frequencies can also be determined by solving the secular equation

$$\det(-\eta\omega^2 \mathbb{1} + \omega\sigma^z + \gamma\mathbf{M}^{-1}\mathcal{H}_{\text{SW}}) = 0. \quad (3)$$

If the calculations are performed around a stable equilibrium state, \mathcal{H}_{SW} is a positive definite operator, and the eigenvalue problem is quasi-Hermitian [46]. This means that all eigenvalues are real, but the left $\langle \mathbf{l}_q |$ and right $|\mathbf{r}_q\rangle$ eigenvectors belonging to the same eigenvalue are not adjoints of each other, but form a biorthogonal system instead, $\langle \mathbf{l}_q | \mathbf{r}_{q'} \rangle = \delta_{qq'}$. Furthermore, the eigenvalues are found in $\pm\omega_q$ pairs due to the particle-hole symmetry of the system, which is represented as $\mathcal{C} = \text{diag}(\sigma^x, -\sigma^x)\mathcal{K}$ in this system, where \mathcal{K} denotes complex conjugation. All eigenvectors have the form $|\mathbf{r}_q\rangle = [\mathbf{v}_q, \omega_q \mathbf{v}_q]$, since the latter components are connected to the spin velocity.

In the following, we consider a ferromagnetic system magnetized along the global z direction, and describe the undamped modes for $\alpha = 0$. The rotational symmetry around the z axis is preserved in the absence of spin-orbit coupling, and the z component of the total angular momentum, $\sum_i L_i^z$, remains a conserved quantity. On the level of spin-wave theory, this is reflected by the absence of pairing terms in the Hamiltonian \mathcal{H}_{SW} , which would couple the first and second components of \mathbf{S}^\perp together. Considering only the S_i^+ sector, two types of excitations may be distinguished in inertial dynamics [47]: precessional excitations performing a counterclockwise rotation around the direction of the total angular momentum, which have $\omega > 0$; and nutational excitations performing a clockwise rotation with $\omega < 0$. These are illustrated in Fig. 1. Due to the different rotational senses, the angular momenta of the excited states also differ: $\sum_i L_i^z > \frac{M_i}{\gamma} \sum_i S_i^z$ for precessional and $\sum_i L_i^z < \frac{M_i}{\gamma} \sum_i S_i^z$ for nutational motion. To observe topological edge modes connecting the precessional

and nutational magnon bands, this conservation of the total angular momentum has to be broken.

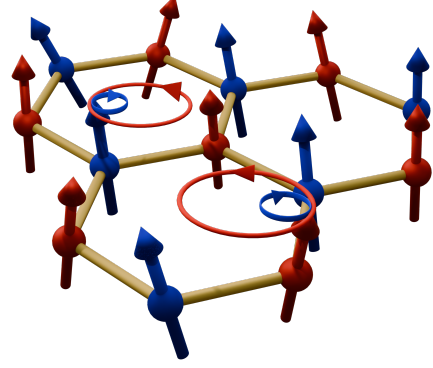


FIG. 1: Sketch of the ferromagnet on the honeycomb lattice. Red and blue trajectories denote counterclockwise precessional and clockwise nutational modes, respectively.

As an example, we consider a ferromagnet on the honeycomb lattice. The Hamiltonian is given by

$$\mathcal{H} = \sum_{\langle i,j \rangle} [S_i^A J_{ij} S_j^B + F (\mathbf{S}_i^A \cdot \hat{\mathbf{r}}_{ij}) (\mathbf{S}_j^B \cdot \hat{\mathbf{r}}_{ij})], \quad (4)$$

where A and B indicate the two sublattices denoted by red and blue spins in Fig. 1, respectively. The exchange interaction tensor J_{ij} between nearest neighbors is diagonal here, with $J^{zz} < J^{xx} = J^{yy} < 0$ preferring magnetization along \hat{z} . The pseudodipolar interaction F connects the spin directions to the relative positions of the sites via the unit vector $\hat{\mathbf{r}}_{ij}$ connecting sites i and j , which is either $\hat{\delta}_1 = (-1, 0)$, $\hat{\delta}_2 = (\frac{1}{2}, -\frac{\sqrt{3}}{2})$, or $\hat{\delta}_3 = (\frac{1}{2}, \frac{\sqrt{3}}{2})$. The parameter values used in the simulations are summarized in Table I.

TABLE I: Dimensionless model parameters used throughout the text.

J^{xx}	J^{zz}	F	γ	η	$M_A = M_B$
-1	-1.1	0.5	1	1	1

The spin-wave Hamiltonian, after spatial Fourier transformation $\mathbf{S}^{A/B,\perp}(\mathbf{k}) = N^{-1/2} \sum_{i/j} e^{-i\mathbf{k}\mathbf{R}_{i/j}} \mathbf{S}_{i/j}^{A/B,\perp}$, may be expressed as

$$\mathcal{H}_{\text{SW}} = \begin{pmatrix} \Omega & \mathcal{H}_1 & 0 & \tilde{F}_1 - i\tilde{F}_2 \\ \mathcal{H}_1^* & \Omega & \tilde{F}_1^* - i\tilde{F}_2^* & 0 \\ 0 & \tilde{F}_1 + i\tilde{F}_2 & \Omega & \mathcal{H}_1 \\ \tilde{F}_1^* + i\tilde{F}_2^* & 0 & \mathcal{H}_1^* & \Omega \end{pmatrix}, \quad (5)$$

where the components are given in the order $[S_-^A, S_-^B, S_+^A, S_+^B]$. The matrix elements are given by

$$\Omega = -3J^{zz}, \quad (6)$$

$$\mathcal{H}_1(\mathbf{k}) = \left(J^{xx} + \frac{F}{2} \right) (e^{i\mathbf{k}\delta_1} + e^{i\mathbf{k}\delta_2} + e^{i\mathbf{k}\delta_3}), \quad (7)$$

$$\tilde{F}_1(\mathbf{k}) = \frac{F}{2} (2e^{i\mathbf{k}\delta_1} - e^{i\mathbf{k}\delta_2} - e^{i\mathbf{k}\delta_3}), \quad (8)$$

$$\tilde{F}_2(\mathbf{k}) = \frac{\sqrt{3}F}{4} (e^{i\mathbf{k}\delta_3} - e^{i\mathbf{k}\delta_2}). \quad (9)$$

The calculated magnon spectrum is shown in Fig. 2 along the high-symmetry lines of the Brillouin zone. The exchange interaction forms two precessional bands in this two-sublattice structure, which touch in the K and K' points forming Dirac cones. Spin inertia leads to additional nutational modes, which have the same dispersion apart from being shifted up in frequency by η^{-1} [17]; see the Supplemental Material [45]. For sufficiently high values of $\eta\gamma M^{-1}|J^{xx}|$, first the top of the higher precession band touches the bottom of the lower nutation band in the Γ point, then a nodal line is formed between the bands along a contour encompassing the Γ point. The pseudodipolar interaction F breaks the continuous rotational symmetry around \hat{z} , thereby causing a hybridization between the precessional and nutational modes and opening gaps in the spectrum. In the Dirac points, the gap is opened for any finite value of F , but its size scales with $|F|^2$, making it difficult to identify in Fig. 2. Along the nodal line, the gap size scales linearly with $|F|$, but this effect can only be observed if the inertial relaxation time is sufficiently high such that the bands overlap. The hybridization between the nutational and precessional bands may be captured by calculating the ellipticity of mode n at wave vector \mathbf{k} ,

$$e_{n,\mathbf{k}} = 2 \langle \mathbf{l}_{n,\mathbf{k}} | P_- | \mathbf{r}_{n,\mathbf{k}} \rangle - 1, \quad (10)$$

where $P_- = \text{diag}(1, 1, 0, 0, 1, 1, 0, 0)$ is the projection onto the clockwise rotating $S_- - V_-$ subspace. The ellipticity takes the value of 1 for left circularly polarized, typically nutational, modes, and -1 for right circularly polarized, typically precessional, modes, while it vanishes for linearly polarized modes forming where the degeneracy along the nodal line is lifted. Alternatively, $e_{n,\mathbf{k}}$ may be thought of as the angular momentum carried by the mode, as discussed above. The avoided crossing may also be detected by studying the polarizations of the modes only in the high-symmetry points: in the Γ point where the right-handed and left-handed modes are eigenstates, the sign of the ellipticity is alternating with increasing energy, while in the M and K points two predominantly right-handed modes are followed by two mainly left-handed modes; see the Supplemental Movies [45].

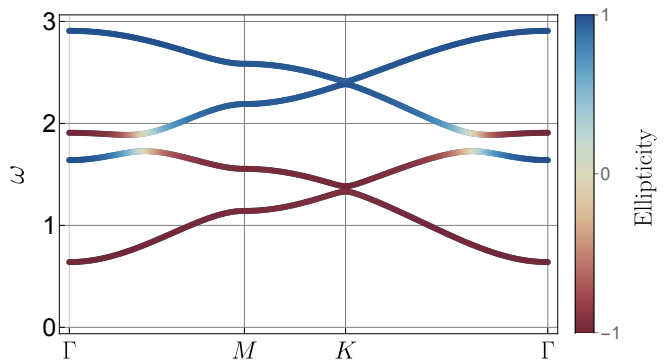


FIG. 2: Magnon band structure in momentum space along high-symmetry points. The states are colored according to their ellipticity defined in Eq. (10).

The gaps opened in the K and K' points have been demonstrated to be topologically non-trivial in this model [40], and this may also be the case for the gap between the precessional and nutational bands. A typical signature of topologically non-trivial gaps is the presence of chiral edge modes at the boundaries [23]. To confirm this bulk-edge correspondence, we recalculated the magnon spectrum in a slab geometry, as shown in Fig. 3. The edge modes are identified by calculating the localization

$$\ell_{n,\mathbf{k}} = \langle \mathbf{l}_{n,\mathbf{k}} | P_{\text{Left}} | \mathbf{r}_{n,\mathbf{k}} \rangle - \langle \mathbf{l}_{n,\mathbf{k}} | P_{\text{Right}} | \mathbf{r}_{n,\mathbf{k}} \rangle, \quad (11)$$

where P_{Left} and P_{Right} are projections onto the sites on the left and right half of the slab, respectively. Close to the Dirac cones where the first and second, respectively the third and fourth bands almost touch, there is a single edge mode crossing the gap. These modes are localized at opposite edges of the system, and propagate in opposite directions based on their group velocity. Chiral edge modes may also be observed between the second and third bands where the avoided crossing between the precessional and nutational bands is found in Fig. 2. While there is a single mode localized on each edge in this gap as well, note that the group velocity changes sign along these modes, with the edge modes having a frequency maximum at the edge of the one-dimensional Brillouin zone. This indicates that the gap between any adjacent pairs of bands is topologically non-trivial. Note that a pair of edge modes is also observable below the lowest magnon band. This is due to the reduced number of neighbors at the edge, which destabilizes the ferromagnetic alignment along the z direction for higher values of the pseudodipolar interaction than what is considered here. However, these edge modes are of topologically trivial origin, and do not merge with the bulk bands as the wave vector varies.

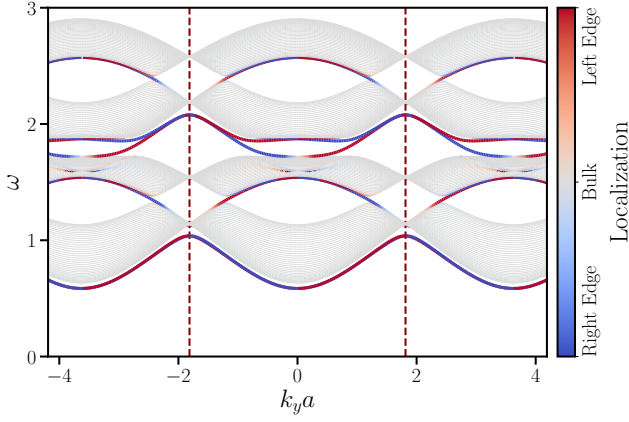


FIG. 3: Magnon band structure in a slab geometry. The system is 40 unit cells wide along the x direction with open boundary conditions, while it is infinite along the y direction with periodic boundary conditions, meaning that the eigenstates can be indexed by the wave vector component k_y . a denotes the distance between nearest-neighbor atoms in the lattice, i.e., the lattice constant is $\sqrt{3}a$. Dotted lines show the boundaries of the one-dimensional Brillouin zone. Coloring shows the localization defined in Eq. (11).

To confirm the topologically non-trivial origin of the edge states, we calculate the topological invariants of the bands in the infinite system, corresponding to the Chern number in the considered case. The Chern number is the integral of the z component of the Berry curvature $C_n = (2\pi)^{-1} \int B_n^z(\mathbf{k}) d^2\mathbf{k}$, where the latter may be expressed with the left and right eigenvectors as (see the Supplemental Material [45] for details)

$$B_n^\alpha(\mathbf{k}) = i\epsilon^{\alpha\beta\gamma} \sum_{m \neq n} \frac{\langle \mathbf{l}_{n,\mathbf{k}} | \partial_{k^\beta} \mathcal{D}_{\mathbf{k}} | \mathbf{r}_{m,\mathbf{k}} \rangle \langle \mathbf{l}_{m,\mathbf{k}} | \partial_{k^\gamma} \mathcal{D}_{\mathbf{k}} | \mathbf{r}_{n,\mathbf{k}} \rangle}{(\omega_{n,\mathbf{k}} - \omega_{m,\mathbf{k}})^2}. \quad (12)$$

Here, $\mathcal{D}_{\mathbf{k}}$ is the matrix on the right-hand side of Eq. (2) in Fourier space, and α, β, γ denote Cartesian indices. The distribution of B_n^z for the four bands is shown in Fig. 4. The sum of the Chern numbers $|\sum_{i=1}^n C_n|$ predicts the number of pair of chiral edge modes between bands n and $n+1$, which equals 1 between any two bands, in agreement with Fig. 3. The Chern number $C_1 = -1$ of the lowest band stems in Fig. 4(a) from the peaks in the Berry curvature close to the K and K' points where the degeneracy is lifted. These peaks are also observable in the second band in Fig. 4(b) with opposite sign, but they are cancelled out by the circular depression around the contour where the precessional and nutational bands overlap in the absence of spin-orbit coupling. The Berry curvatures in the third and fourth bands are qualitatively similar to the second and first bands, respectively, although with reversed signs.

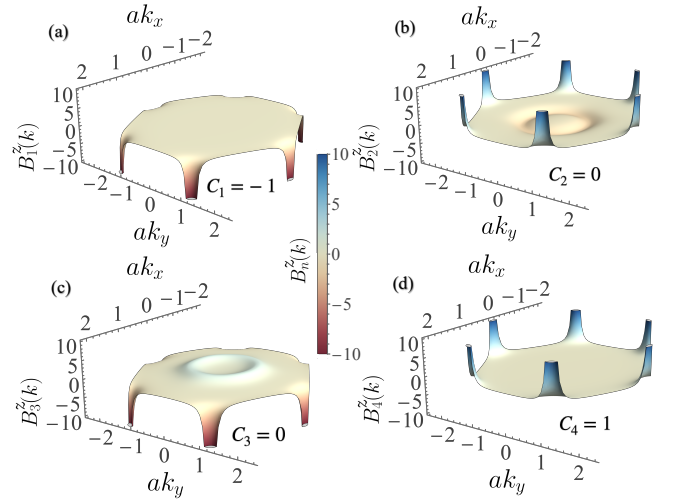


FIG. 4: Berry curvature $B_n^z(\mathbf{k})$ of the bands calculated from Eq. (12). (a)-(d) show the four magnon bands in increasing order of frequency. The Chern numbers C_n for each band are also given.

In summary, we demonstrated that the hybridization between nutational and precessional spin waves in inertial spin dynamics may modify the topological properties of the bands. We illustrated this on the example of a honeycomb ferromagnet, which realizes a magnonic Chern insulator with an avoided crossing between the precessional and nutational bands in the bulk system, which is filled by chiral edge modes in a slab geometry. Assuming an exchange interaction strength of $J \approx -3$ meV and a magnetic moment of $M = 3 \mu_B$, which are in the range of experimentally determined values for honeycomb van der Waals materials [35–37, 48], the inertial relaxation time in the simulations was around $\eta \approx 300$ fs, which is similar to its value determined in transition metals [8, 10]. Note that the value of $|J|$ may be higher in these materials than what was determined from a non-inertial model, since inertial effects considerably reduce the width of the magnon bands [17]; and that the inertial relaxation time may be further enhanced in the presence of heavy elements with high spin-orbit coupling. Therefore, this phenomenon might be observable in experiments.

These effects may be probed by measuring the magnon spectrum in the whole Brillouin zone up to higher energies where the nutational bands are expected to emerge. The nutational and precessional bands may be distinguished based on their different angular momentum, or opposite rotational sense. This means that methods sensitive to the rotational sense of the excitations may be particularly suitable for this purpose, such as spin-polarized electron-energy loss spectroscopy. Optical methods may also be applied in the vicinity of the Γ point where the reversed rotational sense of the higher modes already provides an indication for the topologically non-trivial nature of the bands, as discussed above. Detecting

the inertial dynamics may also shed further light on the role of the competing mechanisms of the Dzyaloshinsky–Moriya interaction and the pseudodipolar interaction in the gap opening in these systems [36, 44]: while the pseudodipolar interaction may open a gap between the precessional and nutational bands, the out-of-plane component of the Dzyaloshinsky–Moriya interaction has no such effect since it preserves the angular momenta of the excitations.

These calculations may be generalized to other systems, for example single-sublattice ferromagnets, where topologically non-trivial bands may only be formed if inertial effects are taken into account; see the Supplemental Material [45] for an example. The generation of bulk and topological edge modes in ferromagnets at THz frequencies may also open further perspectives in controlling the angular-momentum transfer between magnons and phonons or electrons.

A.M. acknowledges funding from the Deutsche Forschungsgemeinschaft (DFG, German Research Foundation) through TRR 173-268565370 (Project B13), and Project No. 504261060 (Emmy Noether Programme), and from the Dynamics and Topology Center (Top-Dyn) funded by the State of Rhineland-Palatinate. R.M. and A.M. acknowledge the Indo-German Science Technology Centre (IGSTC) for the exchange visit via the PECFAR award No. IGSTC/PECFAR/Call 2024/IGSTC-02232/RM-AM/70/2024-25/74. M.C. acknowledges funding from the Deutsche Forschungsgemeinschaft (DFG, German Research Foundation) under the FOR 5844: ChiPS, Project-ID 541503763. L.R. gratefully acknowledges funding by the National Research, Development, and Innovation Office (NRDI) of Hungary under Project Nos. FK142601 and ADVANCED 149745, and by the Hungarian Academy of Sciences via a János Bolyai Research Grant (Grant No. BO/00178/23/11).

-
- [1] H. C. Siegmann, E. L. Garwin, C. Y. Prescott, J. Heidmann, D. Mauri, D. Weller, R. Allenspach, and W. Weber, Magnetism with picosecond field pulses, *J. Magn. Mater.* **151**, L8 (1995).
- [2] E. Beaurepaire, J.-C. Merle, A. Daunois, and J.-Y. Bigot, Ultrafast spin dynamics in ferromagnetic nickel, *Phys. Rev. Lett.* **76**, 4250 (1996).
- [3] T. Kampfrath, A. Kirilyuk, S. Mangin, S. Sharma, and M. Weinelt, Ultrafast and terahertz spintronics: Guest editorial, *Applied Physics Letters* **123**, 10.1063/5.0167151 (2023).
- [4] M.-C. Ciornei, J. M. Rubí, and J.-E. Wegrowe, Magnetization dynamics in the inertial regime: Nutation predicted at short time scales, *Phys. Rev. B* **83**, 020410 (2011).
- [5] H. Suhl, Theory of the magnetic damping constant, *IEEE Trans. Magn.* **34**, 1834 (1998).
- [6] R. Mondal, M. Berritta, A. K. Nandy, and P. M. Oppeneer, Relativistic theory of magnetic inertia in ultrafast spin dynamics, *Phys. Rev. B* **96**, 024425 (2017).
- [7] E. Olive, Y. Lansac, M. Meyer, M. Hayoun, and J.-E. Wegrowe, Deviation from the Landau-Lifshitz-Gilbert equation in the inertial regime of the magnetization, *J. Appl. Phys.* **117**, 213904 (2015).
- [8] R. Mondal, L. Rózsa, M. Farle, P. M. Oppeneer, U. Nowak, and M. Cherkasskii, Inertial effects in ultrafast spin dynamics, *Journal of Magnetism and Magnetic Materials* **579**, 170830 (2023).
- [9] E. Olive, Y. Lansac, and J.-E. Wegrowe, Beyond ferromagnetic resonance: The inertial regime of the magnetization, *Appl. Phys. Lett.* **100**, 192407 (2012).
- [10] K. Neeraj, N. Awari, S. Kovalev, D. Polley, N. Zhou Hagström, S. S. P. K. Arekapudi, A. Semisalova, K. Lenz, B. Green, J.-C. Deinert, *et al.*, Inertial spin dynamics in ferromagnets, *Nature Physics* **17**, 245 (2021).
- [11] V. Unikandanunni, R. Medapalli, M. Asa, E. Albisetti, D. Petti, R. Bertacco, E. E. Fullerton, and S. Bonetti, Inertial spin dynamics in epitaxial cobalt films, *Phys. Rev. Lett.* **129**, 237201 (2022).
- [12] A. De, J. Schlegel, A. Lentfert, L. Scheuer, B. Stadtmüller, P. Pirro, G. von Freymann, U. Nowak, and M. Aeschlimann, Magnetic nutation: Transient separation of magnetization from its angular momentum, *Phys. Rev. B* **111**, 014432 (2025).
- [13] R. Mondal and A. Kamra, Spin pumping at terahertz nutation resonances, *Phys. Rev. B* **104**, 214426 (2021).
- [14] L. Winter, S. Großenbach, U. Nowak, and L. Rózsa, Nutational switching in ferromagnets and antiferromagnets, *Phys. Rev. B* **106**, 214403 (2022).
- [15] R. Rodriguez, M. Cherkasskii, R. Jiang, R. Mondal, A. Etesamirad, A. Tossounian, B. A. Ivanov, and I. Barsukov, Spin inertia and auto-oscillations in ferromagnets, *Phys. Rev. Lett.* **132**, 246701 (2024).
- [16] T. Kikuchi and G. Tatara, Spin dynamics with inertia in metallic ferromagnets, *Phys. Rev. B* **92**, 184410 (2015).
- [17] R. Mondal and L. Rózsa, Inertial spin waves in ferromagnets and antiferromagnets, *Phys. Rev. B* **106**, 134422 (2022).
- [18] M. Cherkasskii, R. Mondal, and L. Rózsa, Inertial spin waves in spin spirals, *Phys. Rev. B* **109**, 184424 (2024).
- [19] M. Cherkasskii, M. Farle, and A. Semisalova, Dispersion relation of nutation surface spin waves in ferromagnets, *Phys. Rev. B* **103**, 174435 (2021).
- [20] P. A. McClarty, Topological magnons: A review, *Annual Review of Condensed Matter Physics* **13**, 171 (2022).
- [21] L. Zhang, J. Ren, J.-S. Wang, and B. Li, Topological magnon insulator in insulating ferromagnet, *Phys. Rev. B* **87**, 144101 (2013).
- [22] A. Mook, J. Henk, and I. Mertig, Magnon hall effect and topology in kagome lattices: A theoretical investigation, *Phys. Rev. B* **89**, 134409 (2014).
- [23] A. Mook, J. Henk, and I. Mertig, Edge states in topological magnon insulators, *Phys. Rev. B* **90**, 024412 (2014).
- [24] R. Chisnell, J. S. Helton, D. E. Freedman, D. K. Singh, R. I. Bewley, D. G. Nocera, and Y. S. Lee, Topological magnon bands in a kagome lattice ferromagnet, *Phys. Rev. Lett.* **115**, 147201 (2015).
- [25] R. Shindou, R. Matsumoto, S. Murakami, and J.-i. Ohe, Topological chiral magnonic edge mode in a magnonic crystal, *Phys. Rev. B* **87**, 174427 (2013).

- [26] A. Roldán-Molina, A. S. Nunez, and J. Fernández-Rossier, Topological spin waves in the atomic-scale magnetic skyrmion crystal, *New Journal of Physics* **18**, 045015 (2016).
- [27] S. A. Díaz, J. Klinovaja, and D. Loss, Topological Magnons and Edge States in Antiferromagnetic Skyrmion Crystals, *Phys. Rev. Lett.* **122**, 187203 (2019).
- [28] T. Weber, D. M. Fobes, J. Waizner, P. Steffens, G. S. Tucker, M. Böhm, L. Beddrich, C. Franz, H. Gabold, R. Bewley, D. Voneshen, M. Skoulatos, R. Georgii, G. Ehlers, A. Bauer, C. Pfeleiderer, P. Böni, M. Janoschek, and M. Garst, Topological magnon band structure of emergent Landau levels in a skyrmion lattice, *Science* **375**, 1025–1030 (2022).
- [29] F.-Y. Li, Y.-D. Li, Y. B. Kim, L. Balents, Y. Yu, and G. Chen, Weyl magnons in breathing pyrochlore antiferromagnets, *Nature Communications* **7**, 10.1038/ncomms12691 (2016).
- [30] A. Mook, J. Henk, and I. Mertig, Tunable magnon weyl points in ferromagnetic pyrochlores, *Phys. Rev. Lett.* **117**, 157204 (2016).
- [31] H. Katsura, N. Nagaosa, and P. A. Lee, Theory of the thermal hall effect in quantum magnets, *Phys. Rev. Lett.* **104**, 066403 (2010).
- [32] R. Matsumoto and S. Murakami, Rotational Motion of Magnon Wave Packet and Berry Curvature, *Phys. Rev. B* **84**, 184406 (2011).
- [33] R. Matsumoto and S. Murakami, Theoretical Prediction of a Rotating Magnon Wave Packet in Ferromagnets, *Phys. Rev. Lett.* **106**, 197202 (2011).
- [34] Y. Onose, T. Ideue, H. Katsura, Y. Shiomi, N. Nagaosa, and Y. Tokura, Observation of the magnon hall effect, *Science* **329**, 297 (2010).
- [35] L. Chen, J.-H. Chung, B. Gao, T. Chen, M. B. Stone, A. I. Kolesnikov, Q. Huang, and P. Dai, Topological Spin Excitations in Honeycomb Ferromagnet CrI₃, *Phys. Rev. X* **8**, 041028 (2018).
- [36] L. Chen, J.-H. Chung, M. B. Stone, A. I. Kolesnikov, B. Winn, V. O. Garlea, D. L. Abernathy, B. Gao, M. Augustin, E. J. G. Santos, and P. Dai, Magnetic Field Effect on Topological Spin Excitations in CrI₃, *Phys. Rev. X* **11**, 031047 (2021).
- [37] F. Zhu, L. Zhang, X. Wang, F. J. dos Santos, J. Song, T. Mueller, K. Schmalzl, W. F. Schmidt, A. Ivanov, J. T. Park, J. Xu, J. Ma, S. Lounis, S. Blügel, Y. Mokrousov, Y. Su, and T. Brückel, Topological magnon insulators in two-dimensional van der Waals ferromagnets CrSiTe₃ and CrGeTe₃: Toward intrinsic gap-tunability, *Science Advances* **7**, 10.1126/sciadv.abi7532 (2021).
- [38] I. Dzyaloshinsky, A thermodynamic theory of “weak” ferromagnetism of antiferromagnetics, *J. Phys. Chem. Solids* **4**, 241 (1958).
- [39] T. Moriya, Anisotropic superexchange interaction and weak ferromagnetism, *Phys. Rev.* **120**, 91 (1960).
- [40] X. S. Wang, Y. Su, and X. R. Wang, Topologically protected unidirectional edge spin waves and beam splitter, *Phys. Rev. B* **95**, 014435 (2017).
- [41] P. A. McClarty, X.-Y. Dong, M. Gohlke, J. G. Rau, F. Pollmann, R. Moessner, and K. Penc, Topological magnons in Kitaev magnets at high fields, *Phys. Rev. B* **98**, 060404 (2018).
- [42] I. Lee, F. G. Utermohlen, D. Weber, K. Hwang, C. Zhang, J. van Tol, J. E. Goldberger, N. Trivedi, and P. C. Hammel, Fundamental Spin Interactions Underlying the Magnetic Anisotropy in the Kitaev Ferromagnet CrI₃, *Phys. Rev. Lett.* **124**, 017201 (2020).
- [43] R. Jaeschke-Ubiergo, E. Suárez Morell, and A. S. Nunez, Theory of magnetism in the van der Waals magnet CrI₃, *Phys. Rev. B* **103**, 174410 (2021).
- [44] V. Brehm, P. Sobieszczyk, J. N. Kløgetvedt, R. F. L. Evans, E. J. G. Santos, and A. Qaiumzadeh, Topological magnon gap engineering in van der Waals CrI₃ ferromagnets, *Phys. Rev. B* **109**, 174425 (2024).
- [45] See Supplemental Material at [URL] for considerations about angular-momentum conservation, the derivation of linear spin-wave theory and the Berry curvature in the inertial regime, and discuss the topological phase transition as a function of the parameters in the honeycomb lattice and the formation of a magnonic Chern insulating state in a single-sublattice ferromagnet. It also contains Refs. [49, 50].
- [46] F. Scholtz, H. Geyer, and F. Hahne, Quasi-hermitian operators in quantum mechanics and the variational principle, *Annals of Physics* **213**, 74–101 (1992).
- [47] R. Mondal, S. Großenbach, L. Rózsa, and U. Nowak, Nutation in antiferromagnetic resonance, *Phys. Rev. B* **103**, 104404 (2021).
- [48] D. Soriano, M. I. Katsnelson, and J. Fernández-Rossier, Magnetic two-dimensional chromium trihalides: A theoretical perspective, *Nano Letters* **20**, 6225–6234 (2020).
- [49] J. Pommier, P. Meyer, G. Pénissard, J. Ferré, P. Bruno, and D. Renard, Magnetization reversal in ultrathin ferromagnetic films with perpendicular anisotropy: Domain observations, *Phys. Rev. Lett.* **65**, 2054 (1990).
- [50] R. Allenspach, M. Stampanoni, and A. Bischof, Magnetic domains in thin epitaxial co/au(111) films, *Phys. Rev. Lett.* **65**, 3344 (1990).